ChemComm

COMMUNICATION

View Article Online
View Journal | View Issue

Cite this: *Chem. Commun.*, 2022, **58**, 13799

Received 16th November 2022,
Accepted 22nd November 2022

DOI: 10.1039/d2cc06204f

rsc.li/chemcomm

Reeling them in: Ph_2PSiMe_3 in the sequential formation of InP magic-sized clusters†

Theodore A. Gazis and Peter D. Matthews *

Indium phosphide magic-sized clusters (MSCs) have been identified as a key step in the growth of InP quantum dots (QDs). However, the need for elevated temperatures to form QDs from MSCs has limited our understanding of this transformation. Herein, we utilize Ph_2PSiMe_3 to identify additional MSC intermediate species, which absorb from 365 nm to 490 nm. Excitingly, particle growth was carried out at 100 °C without the use of acidic surfactants. We show that despite being discrete, stable, and isolable sizes of MSCs, they form a reaction continuum, thus providing further insight into the growth mechanism of InP.

The quantum dot (QD) market is forecast to grow exponentially in the coming years with an expected value of $8.1 billion by 2026.[1] Driving growth in this area is the versatility of these nanomaterials with applications ranging from the conventional (display and lighting solutions) to the innovative (photovoltaics, biomedicine).[2] The high commercial interest, coupled with environmental and health concerns associated with the use of heavy metals in traditional QDs,[3,4] has accelerated the necessity for alternatives. InP QDs are promising candidates as they exhibit similar optical properties to their Cd counterparts whilst being composed of relatively cheap, sustainable, and earth-abundant elements.[4]

However, the exacting synthesis of InP QDs has hampered their widespread adoption.[5] $P(SiMe_3)_3$, the phosphorus precursor of choice, is rapidly consumed during the nucleation phase to form the QD core. Thus, the ensuing growth phase is forced to adhere to an Ostwald ripening process, where nuclei absorb other centers at uneven growth rates. The resultant polydisperse range of QDs absorbs and emits light over a broad range of wavelengths, with limited control.

Previous efforts to temper this reactivity have been met with limited success. Notable examples include changing the alkyl group on the silicon moiety,[7–9] fine-tuning the sequence of chemical addition,[10] using species that are in the wrong oxidation state [*e.g.*, $P(NEt_2)_3$],[11] or employing flow chemistry.[6,12] Recent mechanistic studies, however, have cast doubt on the importance of precursor conversion rate as QD size distribution did not improve for many of these examples.[13–15]

Alternatively, a strategy of particular promise involves the physical separation of nucleation and growth by employing so-called magic-sized clusters (MSC), which are believed to be intermediates in the reaction pathway between In–P monomers and bulk InP QDs.[13,16–19] In these protocols, a lower temperature (60–150 °C) hot injection reaction leads to the formation of stable MSCs (10s–100s of atoms) which are purified and isolated. Subsequently, these are employed as single-source precursor (SSP) seeds to form QDs at higher temperatures. Xie *et al.* pioneered this technique for III-V semiconductors by utilizing InAs and InP MSCs as kinetic probes for QD formation.[20] Major inroads were made by the Cossairt group who isolated and crystallographically characterized the $[In_{37}P_{20}(O_2CR)_{51}]$ (R = CH_2Ph) MSC.[21] Other groups have expanded the scope to other indium sources and identified additional MSC sizes. Notably, when MSCs are applied as single-source precursors for QD synthesis a narrower size distribution is observed in comparison to classical molecular precursors.[17]

All the examples mentioned above relied upon the use of In carboxylates, precursors notorious for being sources of oxygen contaminants.[22] These acids are incompatible with the archetypal P^{3-} precursor, $P(SiMe_3)_3$ as deleterious side reactions with carboxylic acids are widely reported. Replacing the carboxylate ligand set with a phosphonate-based one was recently proposed as a solution.[23] However, the resultant MSCs proved extremely thermally stable (up to 400 °C) thus increasing the cost and difficulty of large-scale production. Furthermore, to colloidally stabilize QDs, fatty acids are commonly introduced into the reaction mixture. At elevated temperatures they are susceptible to ketonization reactions which release H_2O.[24,25]

School of Chemical & Physical Sciences, Keele University, Newcastle-under-Lyme, ST5 5BG, UK. E-mail: p.d.matthews@keele.ac.uk; Tel: +44 (0)1782 733188

† Electronic supplementary information (ESI) available: Experimental protocols, FT-IR and UV-vis spectra, PXRD data (PDF). See DOI: **https://doi.org/10.1039/d2cc06204f**

Consequently, surface oxidation of the highly reactive surface P^{3-} occurs, an irrepressible side reaction. In turn, reaction reproducibility, product homogeneity, and nanoparticle size all suffer, which are some of the core tenets MSCs were developed to govern.[26] Therefore, our group has been searching for ways to remove oxygen-containing species from the reaction mixture completely.

To address these concerns, herein we present a reaction protocol free from acidic reactants. The inclusion of commercially available Ph_2PSiMe_3 as a dopant, conferred sharp excitonic features upon the MSCs. Altering the ratio of Ph_2PSiMe_3 to $P(SiMe_3)_3$ (1–5 equiv.) or the InX_3 source (X = Cl, I, OAc) enabled precise control over the optical properties of the MSCs. Indeed, select examples mirrored the UV signatures of QDs. Remarkably, the above system was receptive to growth at 100 °C using volatile toluene as the reaction solvent. Crucially, the results achieved add another layer of control over InP QD growth under mild reaction conditions.

Our initial experimental studies utilized the hot injection protocol at 100 °C in toluene with excess oleylamine (OAm) as the surfactant and no Ph_2PSiMe_3 present. These conditions were chosen to mimic typical conditions of QD growth at lower temperatures. Upon injection of $P(SiMe_3)_3$ to the $InCl_3$/OAm suspension, a very weak shoulder around λ = 430 nm was barely discernible. Protracted heating failed to resolve further this species (ESI,† Fig. S2).

Previous reports have highlighted the ability of dopants to improve the optoelectronic properties of InP nanoparticles. Taking this into account, the post-synthetic addition of 1 equivalent of Ph_2PSiMe_3 at 100 °C led to a noticeable, albeit weak, size selection effect over the course of 30 minutes (ESI,† Fig S2.6). Encouraged by this result, we repeated the reaction this time co-injecting an equimolar solution of Ph_2PSiMe_3 and $P(SiMe_3)_3$ to the hot $InCl_3$/OAm suspension. This adjustment provided a markedly improved UV spectrum enabling monitoring of the reaction by UV-vis spectroscopy. At the start of the reaction, a short-lived intermediate was present at 386 nm (386-InP), the wavelength previously associated with the Cossairt crystal.[21] Within 15 min a new shoulder gradually emerged at 430 nm (430-InP) and came to dominate the spectrum (Fig. 1). This species proved thermodynamically persistent as no further UV shoulders were observed despite 48 hours of continuous heating at 100 °C.

One of the established hallmarks of MSCs is their thermal stability, with a previous 386-InP example being stable to 400 °C thanks to its phosphonate ligand set.[22] We probed the reactivity of our system by reducing the injection temperature to 70 °C, which proved sufficient to impede conversion to 430-InP. Instead, the absorption peak remained at 386 nm for at least 48 hours at this temperature (ESI,† Fig. S2.6). Pleasingly, upon raising the temperature to 100 °C, a gradual conversion to 430-InP occurred. The process was completed within twenty minutes. The absorption associated with 430-InP grows at the expense of that of 386-InP suggesting these species exist on a continuum of reactivity rather than comprising discrete unrelated species.

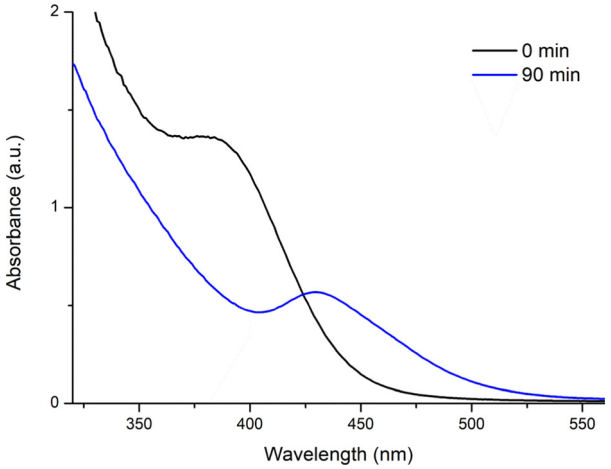

Fig. 1 An equimolar mixture of Ph_2PSiMe_3/$P(SiMe_3)_3$ was added to a 100 °C solution of $InCl_3$ and oleylamine in toluene. The initial formation of 386-InP was followed by conversion to 430-InP which remained stable despite protracted heating.

Most importantly, to the best of our knowledge, this is the first instance of an InP MSC with a UV-vis signature near the 450 nm threshold forming at 100 °C. Consequently, its structure and composition warrant special attention. To this end, the PXRD diffractogram corresponds to bulk InP powder (ESI,† Fig. S2.1), but with some line broadening present due to the small size of the cluster. No In_2O_3 was detectable. We next sought to ascertain if Ph_2PSiMe_3 was incorporated into our MSC. Surface-sensitive attenuated total reflection fourier transform infraRed spectroscopy (ATR-FTIR) measurements of the 430-InP were conducted and compared to oleylamine and Ph_2PSiMe_3 (Fig. 2). A characteristic aryl stretch at 1500–1580 cm^{-1} indicates the inclusion of a diphenylphosphine moiety on the surface of our MSC. To add further credence to this postulate we investigated the clusters through ^1H and NOESY NMR spectroscopy, which demonstrate the presence of broad signals corresponding to the presence of both the

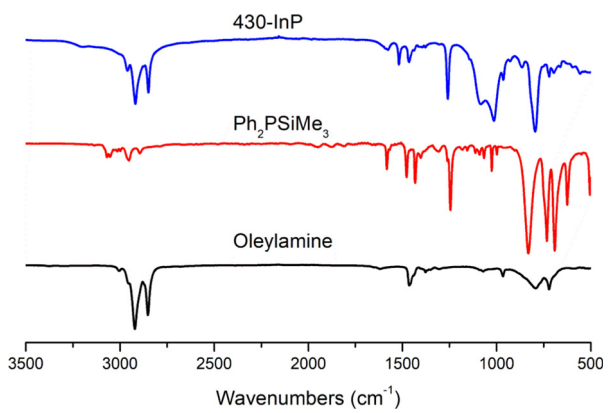

Fig. 2 ATR-FTIR spectra of 430-InP, Ph_2PSiMe_3 and oleylamine (top to bottom) showcasing the presence of an arylphosphine species on the surface of the cluster.

diphenylphosphine moiety and the oleylamine ligands (ESI,† Fig. S2.7 and S2.8).

With insights into the location of Ph_2PSiMe_3 in our cluster, we turned our attention to the mechanistic role of the indium and phosphorus precursors. To begin with, we postulated that adding additional equivalents of Ph_2PSiMe_3 would further redshift the UV signatures. Literature precedence does exist, with the Cossairt group able to continuously redshift their 386-InP MSC to λ = 404 nm with increasing equivalents of arylamines.[28] In this instance, we failed to observe a similar effect despite adding 5 equivalents of Ph_2PSiMe_3 and extended heating for 3 hours. Our system does not appear receptive to post-synthetic modification at 100 °C.

The situation differs when Ph_2PSiMe_3 is included at the start of the reaction. Three new separate reactions were set up with incremental increases of 1.75, 3 and 5 equivalents of Ph_2PSiMe_3. The ratio of all other reaction components was maintained. Pleasingly, new shoulders emerged at 450 nm (1.75 equiv.), 470 nm (3 equiv.) and 490 nm (5 equiv.) respectively (Fig. 3). Most excitingly, absorption at 490 nm is indicative of a QD material, which is unusual to form under such mild conditions. In each case, the MSCs rapidly move through the various smaller-sized MSCs that we have been able to isolate (ESI,† Fig. S2.2). On the other end of the spectrum, reducing the molar ratio of Ph_2PSiMe_3 to 0.1 or 0.5 equivalents does not yield any new species between 386-InP and 430-InP. Instead, it results in slowed-down growth over a longer period (ESI,† Fig. S2.3). Notably, this redshifting of the 430-InP could not be replicated by adding excess $PSiMe_3$ rather than Ph_2PSiMe_3. Instead, the particles crashed out of solution.

We next examined the influence of the indium precursor on the optoelectronic signature. $InCl_3$ was replaced with InI_3, InF_3 and $In(OAc)_3$ in a series of three separate reactions. All other reaction parameters were kept constant. Fig. 4 displays the results obtained. InF_3 was not amenable to this transformation with little apparent dissolution of InF_3 and no MSCs observed even after 48 hours. On the other hand, InI_3 and $In(OAc)_3$ both yielded MSCs. For $In(OAc)_3$ a single shoulder was visible at 430 nm after 1 h. In contrast, InI_3 developed 2 observable shoulders at 365 and 386 nm in a discontinuous manner and grew no further. The rate of conversion was slower compared to the chlorinated congener, with the 365-InP clusters enduring for several minutes prior to converting to the thermodynamically stable product 386-InP. Our findings provide the first tangible link between the 365-InP and 386-InP MSCs, which have separately been reported previously.[19,23,27] Notably, these literature clusters used different precursors and surfactants to our protocol. This growth in discrete jumps is a familiar concept in the more established II–VI QD systems.[29] The sequential conversion of 365-InP to 386-InP (InI_3) and 386-InP to 430-InP for $InCl_3$ extends this principle to InP MSCs for the first time.

Reviewing our experimental observations in their totality has allowed us to put forward a mechanistic hypothesis for our system (Fig. 5). In formulating our understanding, we have taken into account (a) the inclusion of Ph_2PSiMe_3 dramatically improves the excitonic features of InP-430 nm (b) the effect is strongly diminished/non-existent when Ph_2PSiMe_3 is added

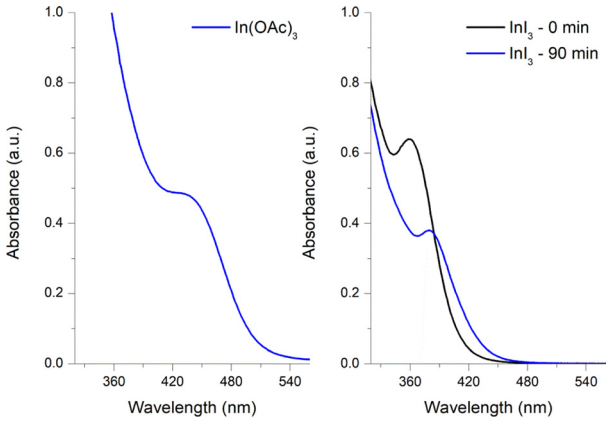

Fig. 4 Altering the indium source to (a) $In(OAc)_3$ gives 430-InP, whilst the use of (b) InI_3 initially gives 365-InP, before leading to clean growth to 386-InP.

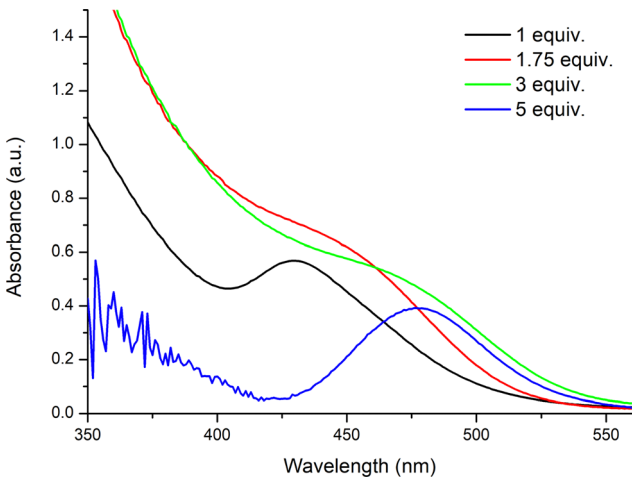

Fig. 3 Increasing the equivalents of Ph_2PSiMe_3 in the reaction mixture facilitates the redshifting of UV signatures.

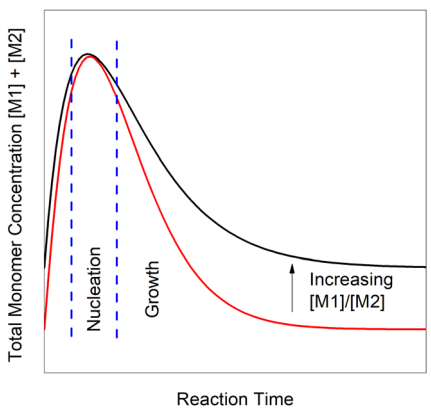

Fig. 5 Increasing the [M1]/[M2] ratio alters the growth phase of MSC formation by providing a well of less reactive monomer species.

post synthetically (c) Ph_2PSiMe_3 is present on the surface of the nanoparticles (d) excess $PSiMe_3$ does not promote growth to InP-490 but rather particle precipitation (e) on the other hand excess Ph_2PSiMe_3 added *in situ* continuously redshifts the UV signatures up to λ = 490 nm and (f) the indium source also affects the absorption characteristics of our MSCs.

It is widely accepted that monomer formation precedes nanoparticle growth in InP systems. We postulate that Ph_2PSiMe_3 forms an InP species (M1) alongside the traditional $P(SiMe_3)_3$–In monomer (M2). The two phosphorus precursors are in direct competition for the same finite Indium source. The more Ph_2PSiMe_3 present at the start of the reaction, the more balance shifts towards M1 formation. The Indium in M1 is far less accessible than free Indium precursor. Thus, it provides temporal segregation between nucleation and growth as it acts as a 'slow-release' reservoir of Indium. Slow diffusion of M1 on the surface of the nanoparticles, as per the La Mer model, leads to the sharper excitonic features and redshifting reported.[30]

Having developed a reproducible protocol for MSC growth, we applied the same technique to direct QD growth using octadecene as the reaction solvent and a hot injection temperature of 200 °C (detailed experimental in ESI†). An equimolar solution of PPh_2SiMe_3/$PSiMe_3$ was utilised. All other reaction parameters remained unchanged. Pleasingly, a shoulder appeared at 580 nm after 30 minutes (ESI,† Fig. S2.4). In an identical manner to the MSCs (*vide supra*), the FTIR spectrum denotes the presence of diphenylphosphine groups on the surface of the QD. Interestingly, repeating the protocol in the absence of Ph_2PSiMe_3 leads to a colloidally unstable precipitate, strongly suggesting the surface-bound Ph_2P groups are aiding in the solvation of the QD. No doubt remains as to the importance of Ph_2PSiMe_3 in our system.

In summary, we have explored the role of Ph_2PSiMe_3 in InP MSC growth at low temperatures. We identified six isolable MSCs and proved their formation proceeds in a sequential fashion. These include literature-reported examples at 365 and 386 nm as well as novel examples at 430 nm, 450 nm, 470 nm, and 490 nm. Control over the observed UV signatures could be exerted by simply tuning the ratio of Ph_2PSiMe_3 to precursors, a desirable feature for industry-based syntheses of QDs. Subsequent studies to better understand the mechanism and role of phosphine dopants in our system are ongoing within our group.

The authors acknowledge the support of EPSRC grant EP/V043412/1 and the UK Government and European Union as contributors to the Smart Energy Network Demonstrator, ERDF project number 32R16P00706 for funding.

Conflicts of interest

There are no conflicts to declare.

Notes and references

1 N. S. Purba and R. Nooraeni, *Proceedings of the International Conference on Trade (ICOT 2019)*, Atlantis Press, 2019, pp. 126–130.
2 M. A. Cotta, *ACS Appl. Nano Mater.*, 2020, **3**, 4920–4924.
3 E. Oh, R. Liu, A. Nel, K. B. Gemill, M. Bilal, Y. Cohen and I. L. Medintz, *Nat. Nanotechnol.*, 2016, **11**, 479–486.
4 G. Xu, S. Zeng, B. Zhang, M. T. Swihart, K. T. Yong and P. N. Prasad, *Chem. Rev.*, 2016, **116**, 12234–12327.
5 S. Tamang, C. Lincheneau, Y. Hermans, S. Jeong and P. Reiss, *Chem. Mater.*, 2016, **28**, 2491–2506.
6 P. Ramasamy, K. J. Ko, J. W. Kang and J. S. Lee, *Chem. Mater.*, 2018, **30**, 3643–3647.
7 H. B. Chandrasiri, E. B. Kim and P. T. Snee, *Inorg. Chem.*, 2020, **59**, 15928–15935.
8 S. Joung, S. Yoon, C. S. Han, Y. Kim and S. Jeong, *Nanoscale Res. Lett.*, 2012, **7**, 93.
9 D. C. Gary, B. A. Glassy and B. M. Cossairt, *Chem. Mater.*, 2014, **26**, 1734–1744.
10 S. Koh, T. Eom, W. D. Kim, K. Lee, D. Lee, Y. K. Lee, H. Kim, W. K. Bae and D. C. Lee, *Chem. Mater.*, 2017, **29**, 6346–6355.
11 M. D. Tessier, K. De Nolf, D. Dupont, D. Sinnaeve, J. De Roo and Z. Hens, *J. Am. Chem. Soc.*, 2016, **138**, 5923–5929.
12 O. B. Achorn, D. Franke and M. G. Bawendi, *Chem. Mater.*, 2020, **32**, 6532–6539.
13 B. M. Cossairt, *Chem. Mater.*, 2016, **28**, 7181–7189.
14 D. Franke, D. K. Harris, L. Xie, K. F. Jensen and M. G. Bawendi, *Angew. Chem., Int. Ed.*, 2015, **54**, 14299–14303.
15 B. M. McMurtry, K. Qian, J. K. Teglasi, A. K. Swarnakar, J. De Roo and J. S. Owen, *Chem. Mater.*, 2020, **32**, 4358–4368.
16 Z. Xu, Y. Li, J. Li, C. Pu, J. Zhou, L. Lv and X. Peng, *Chem. Mater.*, 2019, **31**, 5331–5341.
17 M. R. Friedfeld, D. A. Johnson and B. M. Cossairt, *Inorg. Chem.*, 2019, **58**, 803–810.
18 Y. Kwon and S. Kim, *NPG Asia Mater.*, 2021, **13**, 37.
19 J. Ning and U. Banin, *Chem. Commun.*, 2017, **53**, 2626–2629.
20 L. Xie, Y. Shen, D. Franke, V. Sebastián, M. G. Bawendi and K. F. Jensen, *J. Am. Chem. Soc.*, 2016, **138**, 13469–13472.
21 D. C. Gary, S. E. Flowers, W. Kaminsky, A. Petrone, X. Li and B. M. Cossairt, *J. Am. Chem. Soc.*, 2016, **138**, 1510–1513.
22 K. P. Kepp, *Inorg. Chem.*, 2016, **55**, 9461–9470.
23 D. C. Gary, M. W. Terban, S. J. L. Billinge and B. M. Cossairt, *Chem. Mater.*, 2015, **27**, 1432–1441.
24 D. C. Gary and B. M. Cossairt, *Chem. Mater.*, 2013, **25**, 2463–2469.
25 A. Cros-Gagneux, F. Delpech, C. Nayral, A. Cornejo, Y. Coppel and B. Chaudret, *J. Am. Chem. Soc.*, 2010, **132**, 18147–18157.
26 J. L. Stein, W. M. Holden, A. Venkatesh, M. E. Mundy, A. J. Rossini, G. T. Seidler and B. M. Cossairt, *Chem. Mater.*, 2018, **30**, 6377–6388.
27 R. Xie, Z. Li and X. Peng, *J. Am. Chem. Soc.*, 2009, **131**, 15457–15466.
28 D. C. Gary, A. Petrone, X. Li and B. M. Cossairt, *Chem. Commun.*, 2017, **53**, 161–164.
29 Z. He, D. Wang, Q. Yu, M. Zhang, S. Wang, W. Huang, C. Luan and K. Yu, *ACS Omega*, 2021, **6**, 14458–14466.
30 J. Polte, *CrystEngComm*, 2015, **17**, 6809–6830.

